Available online at www.sciencedirect.com
ScienceDirect
Trans. Nonferrous Met. Soc. China 32(2022) 3478−3486
Transactions of Nonferrous Metals Society of China
www.tnmsc.cn

Theoretical analysis and experimental verification of thermal decomposition mechanism of CuSe

Huan LUO[1,2,3], Heng XIONG[1,2,3,4], Wen-long JIANG[1,2,3,4], Lang LIU[1,2,3], Guo-zheng ZHA[1,2,3,4], Tian-tian ZHEN[1,2,3], Bin YANG[1,2,3,4], Bao-qiang XU[1,2,3,4]

1. National Engineering Research Center of Vacuum Metallurgy, Kunming University of Science and Technology, Kunming 650093, China;
2. Faculty of Metallurgical and Energy Engineering, Kunming University of Science and Technology, Kunming 650093, China;
3. Yunnan Provincial Key Laboratory for Nonferrous Vacuum Metallurgy, Kunming University of Science and Technology, Kunming 650093, China;
4. State Key Laboratory of Complex Non-Ferrous Metal Resources Clean Utilization, Kunming University of Science and Technology, Kunming 650093, China

Received 15 August 2021; accepted 12 April 2022

Abstract: Experiments on the thermal decomposition of CuSe were carried out by using a thermogravimetric analyzer (TGA) at different heating rates. The kinetic parameters and mechanisms were discussed based on model-free and model-based analyses. The decomposition rate and decomposition behavior of CuSe were investigated by using a vacuum thermogravimetric furnace. The results showed that the R3 model was identified as the most probable mechanism function under the present experimental conditions. The average values of activation energy and the pre-exponential factor were 12.344 J/mol and 0.152 s^{-1}, respectively. The actual decomposition rate of CuSe was found to be 0.0030 g/(cm^2·min).

Key words: CuSe; thermal decomposition; non-isothermal kinetics; mechanism

1 Introduction

With the booming development of new semiconductor materials, selenide semiconductors have shown great applications in the fields of biomedicine, photocatalysis, and CuInGaSe thin-film solar cells [1−3]. Notably, CuSe has drawn the attention of many researchers [4−7] owing to its unique and sensitive photovoltaic properties. It is widely used in solar cells [8−11], superionic conductors [12−14], thermoelectric converters, laser infrared detection, photosensitive gas sensor [15], and catalytic degradation [16]. In addition, CuSe serves as an ideal photosensitizer to reduce the probability of occurrence of liver, lung, and prostate cancers [17,18]. Recently, several research methods such as the hydrothermal approach [19], electrochemical synthesis [20], colloidal synthesis [21], solvothermal method [22], and microwave-assisted synthesis have been applied to preparing CuSe. However, the preparation of high purity CuSe is extremely hard because it is easy to decompose to $Cu_{2-x}Se$ [23] by the conventional methods. Therefore, it is especially necessary to study the decomposition properties of CuSe.

Much previous work has shown that CuSe decomposes readily under certain conditions. For example, below 623 K it produces a continuous

Corresponding author: Bao-qiang XU, Tel: +86-13608864121, E-mail: kmxbq@126.com
DOI: 10.1016/S1003-6326(22)66034-5

phase transition from CuSe to $Cu_{2-x}Se$ and then to Cu_2Se [24]. MILMAN [25] predicted that the hexagonal modification of CuSe is less stable than the orthorhombic phase under pressure, and therefore much CuSe exists as an orthorhombic phase in a vacuum environment. LEINEMANN et al [26] determined the enthalpy value of CuSe to be 8 kJ/mol, which corresponded to the enthalpy values of conversion of CuSe to $Cu_{1.8}Se$ and Cu_3Se_2. In the Cu−Se system, Cu_3Se_2, CuSe, and $CuSe_2$ phases decompose at higher temperatures, with only $Cu_{2-x}Se$ and Cu_2Se being stable at 703 K [27]. In general, most scholars have only studied some thermodynamic properties of CuSe. However, none of the studies has provided any details concerning the kinetic mechanism and thermal decomposition behavior of CuSe.

In the present work, experiments on the thermal decomposition of CuSe were carried out at different heating rates by means of a thermogravimetric analyzer (TGA), which has been widely applied in kinetic studies of metallurgy and chemicals [28,29]. The kinetic parameters and mechanisms were detailedly discussed based on the model-free and model-based analyses. The decomposition behavior of CuSe was investigated by a vacuum thermogravimetric furnace. These efforts would contribute to the understanding of the decomposition behavior of CuSe and enrich the database of CuSe decomposition kinetics. In addition, this research could provide much useful information for the preparation process of high-purity CuSe.

2 Experimental

As experimental material, CuSe with the purity of 99.999%, was from Hangzhou Kaiyada Semiconductor Materials Co., Ltd., China, and its chemical composition is listed in Table 1. It can be seen that CuSe contains 0.5×10^{-6} Pb, 1×10^{-6} Fe, 0.5×10^{-6} Sb and a minor amount of Ni, Ag, and Co.

The thermal decomposition experiments were conducted using a TGA (NETZSCH STA 449 C) in a 99.999% argon atmosphere. A 10 mg CuSe sample was heated using a steady stream of Ar (20 mL/min) through a reaction tube. Samples were heated at different heating rates of 5, 10, and 20 K/min, respectively. The kinetic parameters were calculated by increasing the temperature from 298 to 1073 K according to the nonisothermal thermal decomposition experiments of the TGA.

Moreover, a vacuum thermogravimetric furnace (Fig. 1) was employed to measure the actual decomposition rate of CuSe. Then, a crucible containing 20 g CuSe samples was placed in the vacuum furnace and subjected to vacuum pyrolysis experiments at 523 K, 10 Pa, and different time (20, 40, 60, 80, and 100 min). When the target temperature was reached, the temperature was controlled by an automatic control system. The decomposed volatiles (such as Se) with a high saturation vapor pressure would be evaporated and condensed, while residues Cu_2Se remained in the crucible. After decomposition, the crucible and condenser were cleaned and weighed. The phases of materials and samples were detected by an X-ray diffractometer (Mini Flex 600, Japan). The microstructures of samples were characterized by scanning electronic microscopy (SEM). The copper concentrations of samples were detected by inductively coupled plasma-optical emission spectroscopy (ICP-OES).

Table1 Chemical composition of 99.999% CuSe (10^{-6})

Co	Ag	Ni	Pb	Fe	Sb	Si	Hg	Cd	Cu and Se
≤0.2	≤0.2	≤0.2	≤0.5	≤1	≤0.5	≤0.5	≤0.5	≤0.5	Bal.

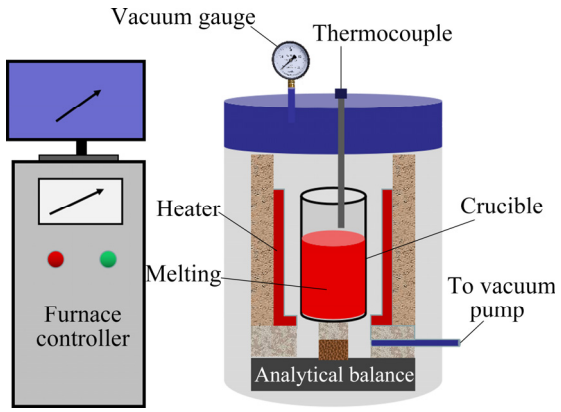

Fig. 1 Schematic diagram of vacuum thermogravimetric furnace

3 Results and discussion

3.1 Thermodynamics of CuSe decomposition

The Gibbs free energy change (ΔG) and the equilibrium compositions of CuSe decomposition reaction were calculated by HSC Chemistry 6.0 software and the results are shown in Fig. 2. From

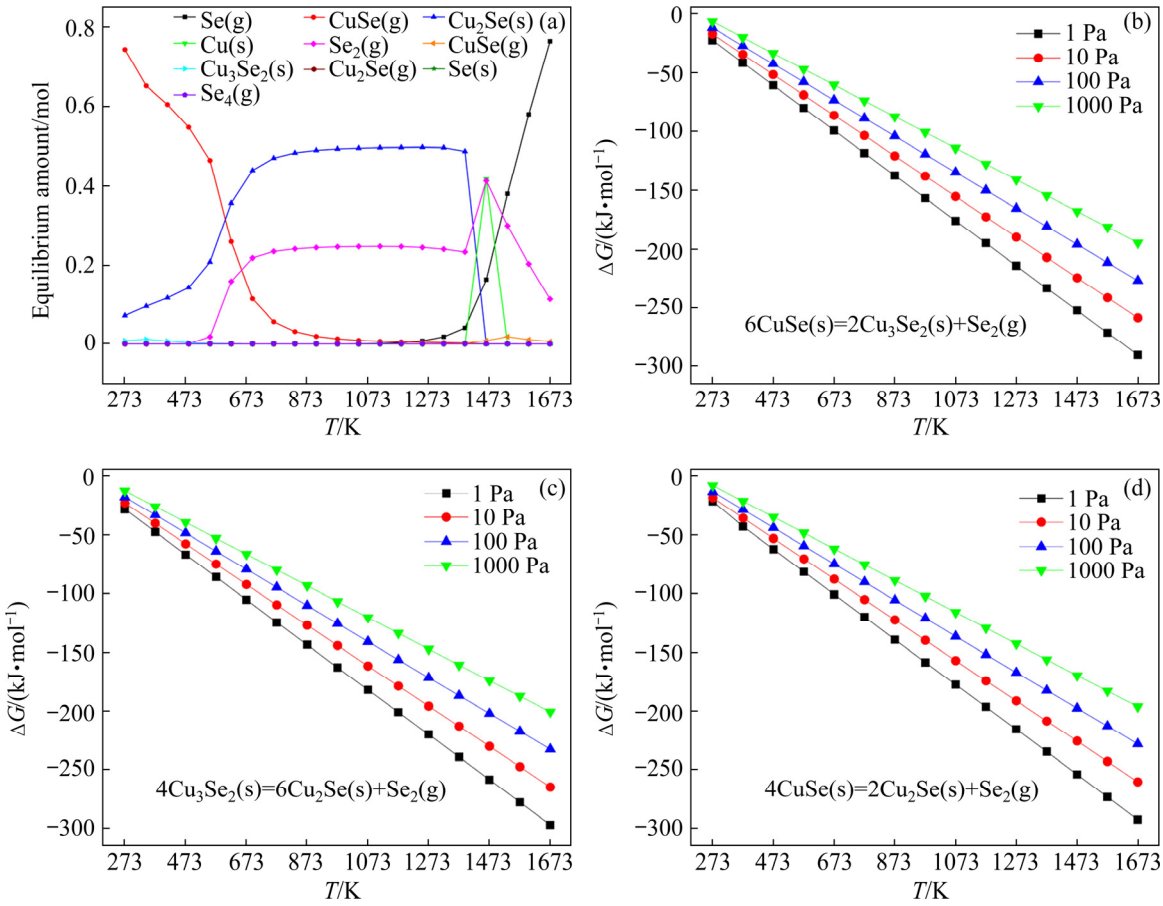

Fig. 2 Theoretical analysis of CuSe: (a) Possible equilibrium composition of CuSe at 273−1673 K; (b−d) Relationship between ΔG and temperature T under different pressures

Fig. 2(a), it can be seen that the amount of CuSe is determined and the possible equilibrium composition in the Cu−Se system is calculated at 273−1673 K. Apparently, the amount of CuSe decreased while Cu_2Se and Se gradually increased at 273−773 K, which was consistent with previous studies [18,24]. The relationships between ΔG and temperature T under different pressures are shown in Figs. 2(b−d). It is evident that the decomposition temperature of CuSe decreases dramatically when the system pressure declines.

3.2 Kinetics of CuSe decomposition

The thermogravimetric (TG) curve and differential thermogravimetric (DTG) curve of the CuSe decomposition process at different heating rates are shown in Fig. 3. Figure 3(a) shows a mass loss of nearly 28.71% in the TG test, which corresponds to the stoichiometric conversion of CuSe to Cu_2Se and Se. Figure 3(b) illustrates that the decomposition process experienced three major stages: an accelerated reaction at the beginning of decomposition, an accelerated reaction over a wide range of temperatures, and a flat reaction at the end of the decomposition. The fastest rates of decomposition reactions at heating rates of 5, 10, and 20 K/min were at 713.5, 740.2 and 770.0 K, respectively.

To describe the kinetic mechanism of solid-state decomposition reactions, integral and differential methods are usually available. The reaction rate is generally expressed as Eq. (1):

$$\frac{\mathrm{d}\alpha}{\mathrm{d}t}=kf(\alpha) \tag{1}$$

$$G(\alpha)=k(t) \tag{2}$$

where α is the conversion rate; $f(\alpha)$ and $G(\alpha)$ are the differential and integral forms of the dynamic mechanism function, respectively [30]. $f(\alpha)$ represents the reaction mechanism function, and $f(\alpha)=1/G(\alpha)$; k is the rate constant (s^{-1}).

$$\alpha=\frac{m_0-m_t}{m_0-m_c} \tag{3}$$

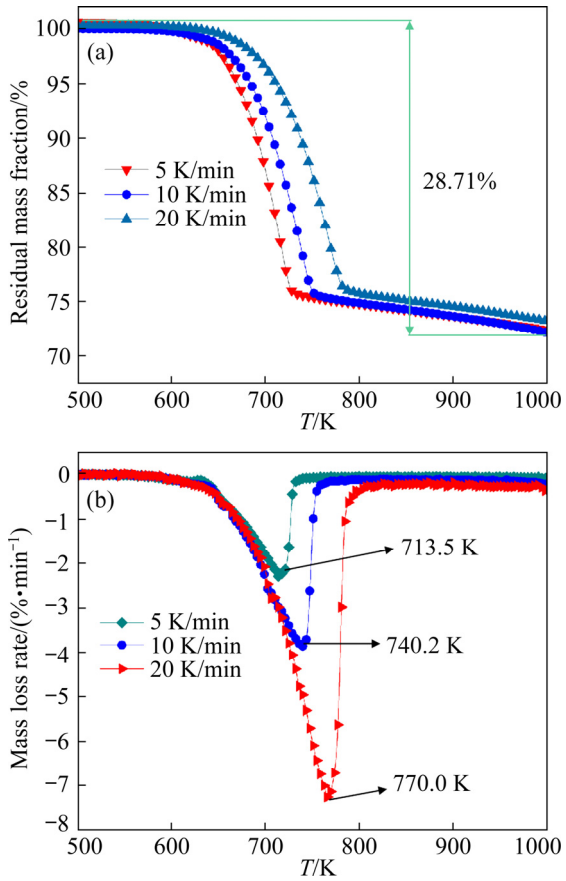

Fig. 3 TG curves (a) and DTG curves (b) of CuSe decomposition process at various heating rates

where m_0 is the initial sample mass, m_t is the sample mass at time t, and m_c is the sample mass after complete conversion from CuSe to Cu_2Se and Se.

The conversion degree (from CuSe to Cu_2Se and Se) could be obtained with Eq. (3) during the thermal decomposition process, which varies between 0 and 1. The Arrhenius equation gives the temperature dependence of the rate constant as shown in Eq. (4):

$$k=A\exp[-E/(RT)] \tag{4}$$

where A is the pre-exponential factor (s^{-1}), E is the activation energy (kJ/mol), and R is the molar gas constant (8.314 J/(mol·K)). Under a certain heating rate β (K/min), Eq. (1) could be transformed to Eq. (5):

$$\frac{\mathrm{d}\alpha}{\mathrm{d}t}=\frac{A}{\beta}\exp[-E/(RT)]\cdot f(\alpha) \tag{5}$$

The conversion rate curves for the thermal decomposition of CuSe at different heating rates are shown in Fig. 4. Slower heating rates and longer reaction time led to higher conversion rates. Initially, the thermal conversion was relatively slow and then gradually increased. When the conversion rates were in the range of 0 to 0.1 and 0.9 to 1, the initial and end stages of the reaction, both had negligible amounts of decomposition. The conversion rate increased linearly between 0.1 and 0.9, which was considered to be the main reaction period for the decomposition of CuSe.

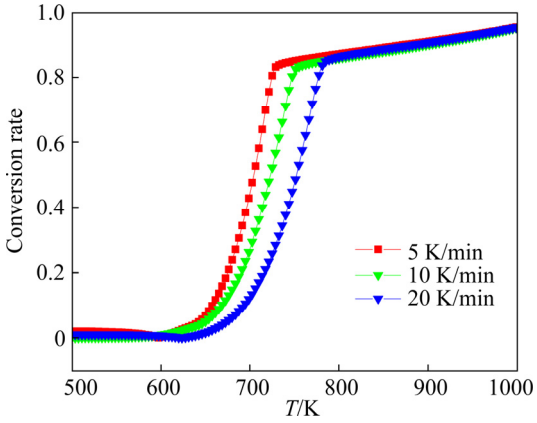

Fig. 4 Conversion rate curves of CuSe thermal decomposition at different heating rates

3.2.1 Model-free analysis

The kinetic parameters for the decomposition of CuSe are determined by Kissinger−Akahira−Sunose (KAS), Flynn−wall Ozawa (FWO), and the Coats−Redfern methods. The KAS method was used to calculate the apparent activation energy (E) for the reaction under multi-temperature conditions [31]. Based on these parameters, the kinetic equation can be expressed as

$$\ln\left(\frac{\beta}{T_p^2}\right)=\ln\left(\frac{AR}{E}\right)-\frac{E}{R}\frac{1}{T_p} \tag{6}$$

The peak temperature of T_p was obtained by DTG curves at different heating rates. This value was substituted into Eq. (6) and the fitted results are shown in Fig. 5 (KAS). The linear correlation coefficient for the regression equation (R^2) was 0.99918, and the formula is as follows:

$$\ln\left(\frac{\beta}{T_p^2}\right)=\ln\left(\frac{AR}{E}\right)-\frac{E}{R}\frac{1}{T_p}=6.27146-1.27081\frac{1}{T_p} \tag{7}$$

According to the regression of Eq. (7) (KAS), the activation energy E for the decomposition of CuSe was 10.567 J/mol. The activation energy E was obtained by the KAS method and verified via the FWO equation. The peak temperature T_p in the

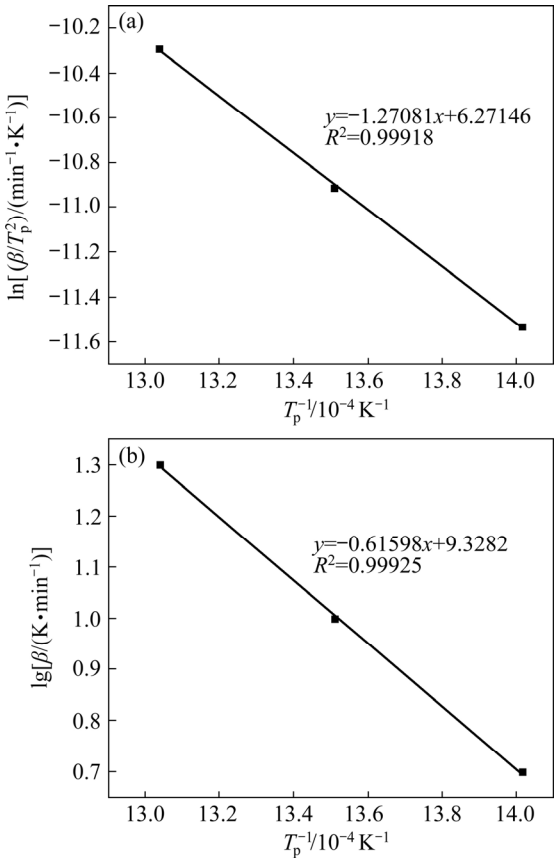

Fig. 5 Thermodynamic equation fitting curves by different models: (a) KAS; (b) FWO

KAS equation was used to replace temperature T in Eq. (8) (FWO method), and linear fitting results are shown in Fig. 5. When the heating rate β is fixed, the values of the activation energy and pre-exponential factor can be obtained by plotting $\lg\beta$ versus T^{-1} (FWO method) with a linear correlation coefficient of 0.99925 for the regression equation as follows:

$$\lg\beta=\lg\frac{AE}{RG(\alpha)}-2.315-0.4567\frac{E}{RT}=$$
$$9.3282-0.61598\frac{1}{T} \quad (8)$$

The average value of activation energy determined by the FWO method was 11.214 J/mol. The FWO method was used to ascertain kinetic parameters with the kinetic mechanism function shown in Eq. (8). The activation energy calculated by the KAS method (E_K) was slightly lower than that of the FWO method (E_F). The results are as follows: $(E_F-E_K)/E_F=0.0577\leq 0.1$. It is verified that the activation energy calculated by the KAS method is highly reliable.

3.2.2 Model-base analysis

To verify the above calculations, the Coats−Redfern method was used as a modularized function method, and shown by Eq. (9), the plot of $\ln(G(\alpha)/T^2)$ versus T^{-1} gives the activation energy and pre-exponential factor for different reaction conditions from the slope and intercept of the curve, respectively.

$$\ln\left[\frac{G(\alpha)}{T^2}\right]=\ln\left[\frac{AR}{\beta E}\left(1-\frac{2RT}{E}\right)\right]-\frac{E}{RT} \quad (9)$$

According to Eq. (9), if the reaction mechanism function is correctly selected, $\ln[G(\alpha)/T^2]$ and T^{-1} should have a linear relationship. The expressions of various reaction mechanism functions were substituted into Eq. (9).

TG and DTG data were employed to build $\ln[G(\alpha)/T^2]-T^{-1}$ curve as shown in Fig. 6. Table 2 summarizes the reaction rate expressions and the corresponding linear correlation coefficients for various mechanistic models. It illustrated that the correlation coefficients for the reaction-order models R3 and D3 are the closest to 1. However, the activation energy calculated for the R3 model is 13.199 J/mol, which is closer to the above calculation results by KAS and FWO. Therefore, the reaction-order model R3 is the most likely mechanism function under the present experimental conditions. The calculated values of activation energy and pre-exponential factor values at different heating rates are presented in Table 3.

The kinetic model and parameters derived from the Coats–Redfern method were combined with the data in Table 3, thus the kinetic equation can be expressed as

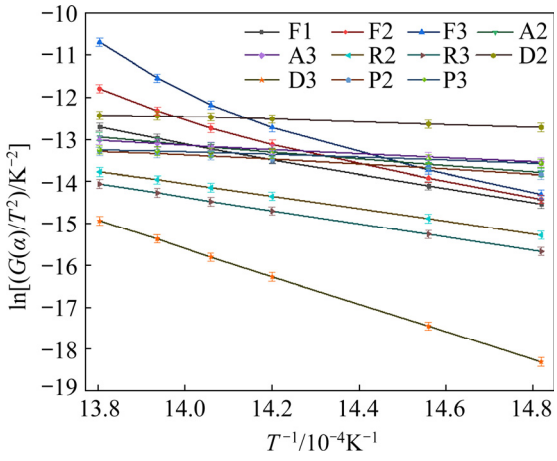

Fig. 6 Curves of $\ln[G(\alpha)/T^2]$ versus T^{-1} at heating rate of 5 K/min

Table 2 Solid-state reaction rate expressions and correlation coefficients for different reaction models

Reaction model	Differential form $f(\alpha)$	Integral form $G(\alpha)$	Correlation coefficient
First-order model (F1)	$1-\alpha$	$-\ln(1-\alpha)$	0.9978
Second-order model (F2)	$(1-\alpha)^2$	$(1-\alpha)^{-1}-1$	0.97893
Third-order model (F3)	$(1-\alpha)^3$	$[(1-\alpha)^{-2}-1]/2$	0.95331
Avarami−Erofe'ev (A2)	$2(1-\alpha)[-\ln(1-\alpha)]^{1/2}$	$[-\ln(1-\alpha)]^{1/2}$	0.99749
Avarami−Erofe'ev (A3)	$3(1-\alpha)[-\ln(1-\alpha)]^{2/3}$	$[-\ln(1-\alpha)]^{1/3}$	0.99711
2D-contraction model (R2)	$2(1-\alpha)^{1/2}$	$1-(1-\alpha)^{1/2}$	0.9998
3D-contraction model (R3)	$3(1-\alpha)^{2/3}$	$1-(1-\alpha)^{1/3}$	0.99987
2D-diffusion model (D2)	$[-\ln(1-\alpha)]^{-1}$	$(1-\alpha)\ln(1-\alpha)+\alpha$	0.98109
3D-diffusion model (D3)	$(3/2)(1-\alpha)^{2/3}[1-(1-\alpha)^{1/3}]^{-1}$	$[1-(1-\alpha)^{1/3}]^2$	0.99987
Power law (P2)	$2\alpha^{1/2}$	$\alpha^{1/2}$	0.99304
Power law (P3)	$3\alpha^{2/3}$	$\alpha^{1/3}$	0.99059

Table 3 Activation energy and pre-exponential factor by Coats−Redfern method

β/(K·min^{-1})	E/(J·mol^{-1})	A/s^{-1}
5	13.199	−0.387
10	11.856	−0.034
20	11.976	−0.035
Average value	12.344	0.152

$$\frac{\mathrm{d}\alpha}{\mathrm{d}t}=0.456\exp\left(\frac{-1.485}{T}\right)(1-\alpha)^{2/3} \tag{10}$$

From kinetic analysis, changing the heating rate will result in a variation of the activation energy of the CuSe decomposition. The kinetic parameters are as follows: activation energy of 12.344 J/mol and pre-exponential factor of 0.152 s^{-1}.

3.3 Thermal decomposition experiments of CuSe

According to thermodynamic calculations, the thermal decomposition experiments of CuSe were carried out at 523 K and 10 Pa. The evaporation resistance of Se is neglected during the vacuum thermal decomposition of CuSe. Hence, the evaporation rate of Se is approximately equal to the conversion rate of CuSe. In this process, slight variations in mass, pressure, and temperature can be recorded by the balance system, and their signals are transmitted to the computer terminal. The actual experimental conversion rate of CuSe will be found by measuring the mass change of CuSe per unit time and area during the actual decomposition process. Theoretical maximum evaporation rate of Se at 523 K is calculated to be 0.0497 g/(cm^2·min) by the Langmuir−Knudsen equation [32]. Finally, the time stability range of 200−2200 s with mass can be linearly fit to obtain reaction rate k_{exp} as shown in Fig. 7 and the experimental decomposition rate at 523 K was directly calculated to be 0.0030 g/(cm^2·min) using the following formula:

$$\omega_{cal}=2.624\times10^{-2}\alpha_1 p^*\sqrt{\frac{M}{T}} \tag{11}$$

$$\omega_{exp}=\frac{\Delta m}{\Delta t S}=\frac{k_{exp}}{S} \tag{12}$$

where ω_{cal} is the theoretical decomposition rate in g/(cm^2·min); α_1 is the accommodation coefficient; $p*$ is the saturation vapor pressure of 5.01 Pa; M is the relative molecular mass of 78.96; T is the melt surface temperature of 523 K; ω_{exp} is the experimental actual decomposition rate of CuSe and represents the mass change (Δm) of CuSe in a certain time (Δt) and area (S=7.065 cm^2).

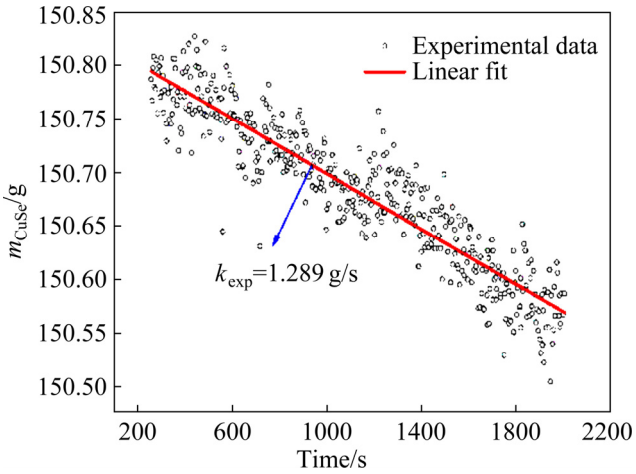

Fig. 7 Linear fitting results for experimental value of k_{exp} at 523 K

Meanwhile, vacuum thermal decomposition experiments were conducted at 523 K, 10 Pa, and 20, 40, 60, 80, and 100 min, respectively, and the results are shown in Fig. 8. It can be seen that the volatile rate of Se increased from 2.4% to 6.5% from 20 to 100 min and that Se contained a certain amount of Cu, fluctuating between 32×10^{-6}–270×10^{-6}. The reason for this result could be that Cu_2Se enters the condensate together with Se due to the adjacent saturation vapor pressure [33]. The results of XRD (Fig. 9) and SEM (Fig. 10) show that CuSe was decomposed into Cu_2Se and Se under the conditions of 523 K, 100 min, and 10 Pa.

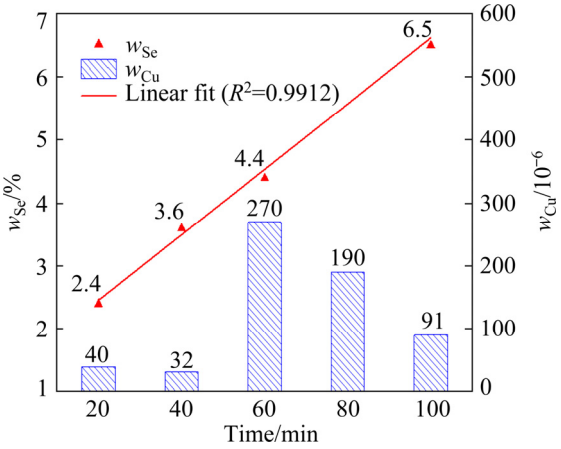

Fig. 8 Relationship between volatile rate of Se (w_{Se}), copper content (w_{Cu}), and time during decomposition of CuSe at 523 K

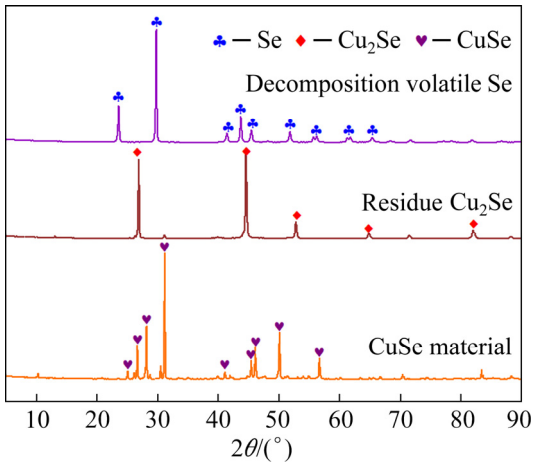

Fig. 9 XRD patterns of CuSe material and decomposition residues and volatiles at 523 K, 100 min, and 10 Pa

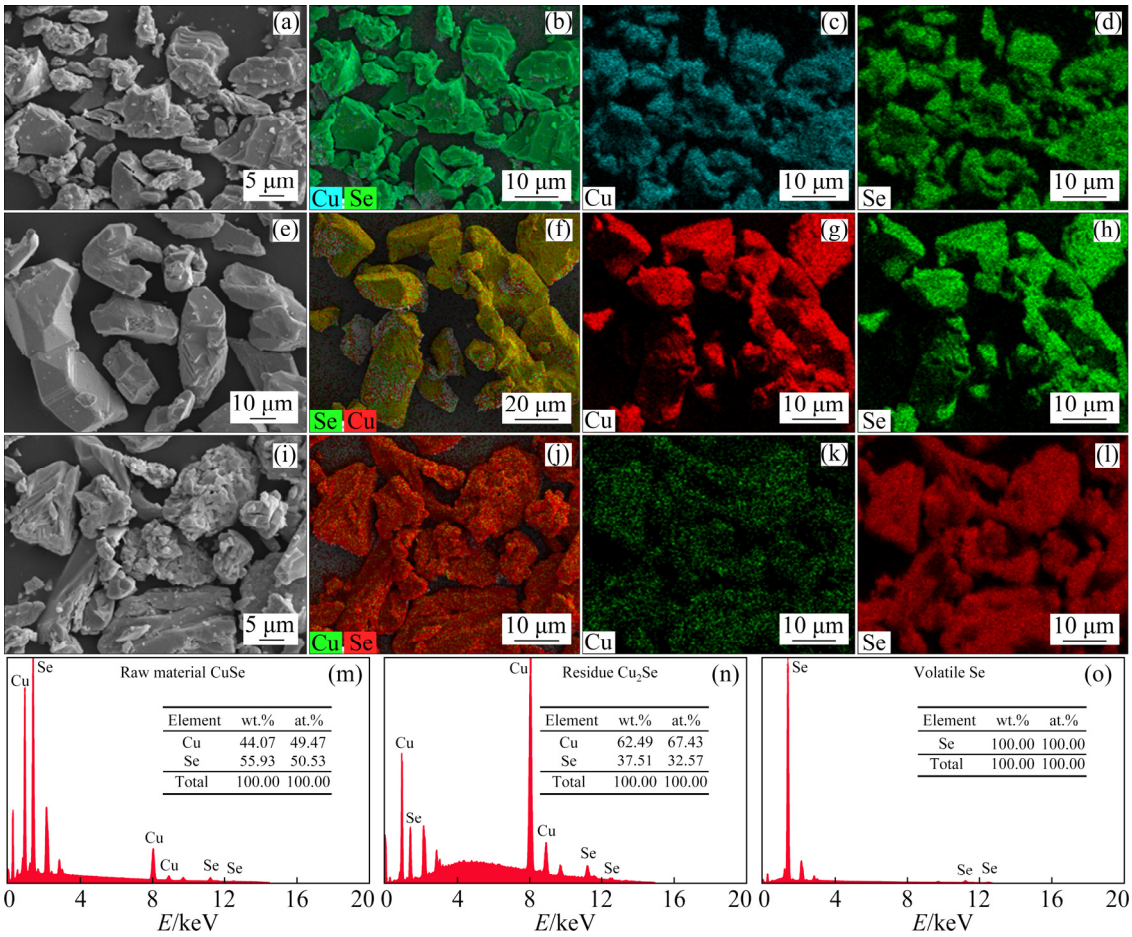

Fig. 10 SEM images (a–l) and EDS results (m–o) of CuSe raw material (a–d), decomposition residues (e–h) and volatiles (i–l) at 523 K, 100 min, and 10 Pa

4 Conclusions

(1) Thermal decomposition kinetic parameters and mechanism of CuSe were discussed based on model-free and model-based analyses. The results showed that the R3 model was identified as the most probable mechanism function under the present experimental conditions. The average values of activation energy and the pre-exponential factor were 12.344 J/mol and 0.152 s^{-1}, respectively. The kinetic equation was obtained. The actual decomposition rate of CuSe was found to be 0.0030 g/(cm^2·min).

(2) The vacuum thermal decomposition experiments of CuSe were conducted, and the results indicated that CuSe decomposed into Cu_2Se and Se by vacuum decomposition under the condition of 523 K, 100 min, and 10 Pa, which was consistent with the thermodynamic calculation results.

Acknowledgments

This work was financially supported by the Basic Research Plan of Yunnan Province, China (No. 2019FA020), the Yunling Scholars of Yunnan Province, China (No. KKRC201952012), the Leading Talents of Industrial Technology in Ten Thousand Talents Plan of Yunnan Province, China, and the Scientist Studio of Yunnan Province, China.

References

[1] CHEN Kai, WANG Xiu-juan, WANG Gang, WANG Bei-bei, LIU Xiao-jie, BAI Jin-tao, WANG Hui. A new generation of high-performance anode materials with semiconductor heterojunction structure of SnSe/SnO_2@Gr in lithium-ion batteries [J]. Chemical Engineering Journal, 2018, 347: 552−562.

[2] GAO Shi-qian, LI Tian-yu, GUO Ye, SUN Chen-xing, XIAN YU Ban-ruo, XU Hua-ping. Selenium-containing nanoparticles combine the NK cells mediated immunotherapy with radiotherapy and chemotherapy [J]. Advanced Materials, 2020, 32: e1907568.

[3] LI Zhan-yu, WANG Xiao-Xu, ZHANG Wen-ming, YANG Shao-peng. Two-dimensional Ti_3C_2@CTAB-Se (MXene) composite cathode material for high-performance rechargeable aluminum batteries [J]. Chemical Engineering Journal, 2020, 398: 125679.

[4] TAKAHASHI T, YAMAMOTO O, MATSUYAMA F, NODA Y. Ionic conductivity and coulometric titration of copper selenide [J]. Journal of Solid State Chemistry, 1976, 16: 35−39.

[5] OKIMURA H, MATSUMAE T, MAKABE R. Electrical properties of $Cu_{2-x}Se$ thin films and their application for solar cells [J]. Thin Solid Films, 1980, 71: 53−59.

[6] RIHA S C, JOHNSON D C, PRIETO A L. Cu_2Se nanoparticles with tunable electronic properties due to a controlled solid-state phase transition driven by copper oxidation and cationic conduction [J]. Journal of the American Chemical Society, 2011, 133: 1383−1390.

[7] CAO Hong-liang, GONG Qiang, QIAN Xue-feng, WANG Hui-li, ZAI Jian-tao, ZHU Zi-kang. Synthesis of 3-D hierarchical dendrites of lead chalcogenides in large scale via microwave-assistant method [J]. Crystal Growth & Design, 2007, 7: 425−429.

[8] NISHIWAKI S, SATOH T, HAYASHI S, HASHIMOTO Y, SHIMAKAWA S, NEGAMI T, WADA T. Preparation of Cu(In,Ga)Se_2 thin films from Cu−Se/In−Ga−Se precursors for high-efficiency solar cells [J]. Solar Energy Materials and Solar Cells, 2001, 67: 217−223.

[9] KOZYTSKIY A V, STROYUK O L, KUCHMIY S Y. Inorganic photoelectrochemical solar cells based on nanocrystalline ZnO/ZnSe and ZnO/CuSe heterostructures [J]. Catalysis Today, 2014, 230: 227−233.

[10] MOLOTO N, PUGGENS H, GOVINDRAJU S, RAKGALAKANE B, KALENGA M. Schottky solar cells: Anisotropic versus isotropic CuSe nanocrystals [J]. Thin Solid Films, 2013, 531: 446−450.

[11] BO Fan, ZHANG Chu-fan, WANG Chun-lei, XU Shu-hong, WANG Zhu-yuan, CUI Yi-ping. From red selenium to cuprous selenide: A novel and facile route to a high-performance metal selenide cathode for sensitized solar cells [J]. Journal of Materials Chemistry A, 2014, 2: 14585−14592.

[12] HORYATIC V, VUCIC Z, MILAT O. Dilatometric study of the anisotropy in the superionic cuprous selenide [J]. Journal of Physics C: Solid State Physics, 1982, 15: L957−L960.

[13] OGORELEC Z, ČELUSTKA B. On the relation between electrical conductivity and phase transition of non-stoichiometric cuprous selenides [J]. Journal of Physics and Chemistry of Solids, 1969, 30: 149−155.

[14] SHOJAEI A R. Electrical conductivity plus probability of superconductivity in α-CuSe/klockmannite, bulk and nano-layers [J]. Journal of Alloys and Compounds, 2015, 632: 568−574.

[15] WANG Zheng-hua, PENG Fei, WU Yi-chun, YANG Li, ZHANG Feng-wei, HUANG Jia-rui. Template synthesis of $Cu_{2-x}Se$ nanoboxes and their gas sensing properties [J] CrystEngComm, 2012, 14: 3528−3533.

[16] LIU Su-li, ZHANG Zeng-song, BAO Jian-chun. Controllable synthesis of tetragonal and cubic phase Cu_2Se nanowires assembled by small nanocubes and their electrocatalytic performance for oxygen reduction reaction [J]. The Journal of Physical Chemistry C, 2013, 117: 15164−15173.

[17] HESSEL C M, PATTANI V P, RASCH M, PANTHANI M G, KOO B, TUNNELL J W, KORGEL B A. Copper selenide nanocrystals for photothermal therapy [J]. Nano Letters, 2011, 11: 2560−2566.

[18] KUMAR P, SINGH K, SRIVASTAVA O N. Template free-solvothermaly synthesized copper selenide (CuSe,

$Cu_{2-x}Se$, β-Cu_2Se and Cu_2Se) hexagonal nanoplates from different precursors at low temperature [J]. Journal of Crystal Growth, 2010, 312: 2804−2813.

[19] GU Yan-jie, SU Yan-jie, CHEN Da, GENG Hui-juan, LI Zhong-li, ZHANG Lu-yin, ZHANG Ya-fei. Hydrothermal synthesis of hexagonal CuSe nanoflakes with excellent sunlight-driven photocatalytic activity [J]. CrystEngComm, 2014, 16: 9185−9190.

[20] JAGMINAS A, JUŠKĖNAS R, GAILIŪTĖ I, STATKUTĖ G, TOMAŠIŪNAS R. Electrochemical synthesis and optical characterization of copper selenide nanowire arrays within the alumina pores [J]. Journal of Crystal Growth, 2006, 294: 343−348.

[21] SERGEY V, FRANCESCO D S, LUCA C, SALDANHA P L, ALICE S, DANG Z Y, ROMAN K, LIBERATO M, VLADIMIR L. Fully solution-processed conductive films based on colloidal copper selenide nanosheets for flexible electronics [J]. Advanced Functional Materials, 2016, 26: 3670−3677.

[22] SONIA S, KUMAR P S, MANGALARAJ D, PONPANDIAN N, VISWANATHAN C. Influence of growth and photocatalytic properties of copper selenide (CuSe) nanoparticles using reflux condensation method [J]. Applied Surface Science, 2013, 283: 802−807.

[23] IBRAHIM G S, ZAINAL A T, JOSEPHINE YING C L, MOHD MUSTAPHA A K, HUSSEIN B, HAN K L, AMINU M. Facile microwave-assisted synthesis and characterization of CuSe nanosheets: Effect of EDTA concentration [J]. Journal of Materials Science Materials in Electronics, 2020, 31: 13549−13560.

[24] SHAFIZADE R B, IVANOVA I V, KAZINETS M M. Electron diffraction study of phase transformations of the compound CuSe [J]. Thin Solid Films, 1978, 55: 211−220.

[25] MILMAN V. Klockmannite, CuSe: Structure, properties and phase stability from ab initio modeling [J]. Acta Crystallographica, 2002, 58: 437−447.

[26] LEINEMANN I, TIMMO K, GROSSBERG M, KALJUVEE T, TÕNSUAADU K, TRAKSMAA R, ALTOSAAR M, MEISSNER D. Reaction enthalpies of $Cu_2ZnSnSe_4$ synthesis in KI [J]. Journal of Thermal Analysis and Calorimetry, 2015, 119: 1555−1564.

[27] SINGH M, BHAN S. Phase equilibria and crystal chemical relations in copper-nickel-selenium system [J]. Progress in Crystal Growth and Characterization of Materials, 1990, 20: 217−230.

[28] CHE Yu-si, HAO Zhen-hua, ZHU Jin-peng, FU Zhen-hua, HE Ji-lin, SONG Jian-xun. Kinetic mechanism of magnesium production by silicothermy in argon flowing [J]. Thermochimica Acta, 2019, 681: 178397.

[29] CHE Yu-si, MAI Geng-peng, LI Shao-Long, HE Ji-lin, SONG Jian-xun, YI Jian-hong. Kinetic mechanism of magnesium production by silicothermic reduction of CaO·MgO in vacuum [J]. Transactions of Nonferrous Metals Society of China, 2020, 30: 2812−2822.

[30] LIU Wei-zao, HU Jin-peng, LIU Qing-cai, LI Chun. Roasting kinetics of ammonium sulfate and calcium titanate [J]. Chemical Industry and Engineering Progress, 2021(8): 7. (in Chinese)

[31] CHEN Yu-jie, WANG Yun-yan, PENG Ning, LIANG Yan-jie, PENG Bing. Isothermal reduction kinetics of zinc calcine under carbon monoxide [J]. Transactions of Nonferrous Metals Society of China, 2020, 30: 2274−2282.

[32] ZHA Guo-zheng, WANG Yun-ke, CHENG Min-qiang, HUANG Da-xin, JIANG Wen-long, XU Bao-qiang, YANG Bin. Purification of crude selenium by vacuum distillation and analysis [J]. Journal of Materials Research and Technology, 2020, 9: 2926−2933.

[33] ZHA Guo-zheng, YANG Bin, LUO Huan, HUANG Da-xin, JIANG Wen-long, XU Bao-qiang, LIU Da-chun. Innovative green approach for the selective extraction of high-purity selenium from hazardous selenium sludge [J]. Separation and Purification Technology, 2021, 266: 118536.

CuSe 热分解机理的热力学计算和实验验证

罗 欢[1,2,3]，熊 恒[1,2,3,4]，蒋文龙[1,2,3,4]，刘 浪[1,2,3]，查国正[1,2,3,4]，甄甜甜[1,2,3]，杨 斌[1,2,3,4]，徐宝强[1,2,3,4]

1. 昆明理工大学 真空冶金国家工程研究中心 昆明 650093；
2. 昆明理工大学 冶金与能源工程学院，昆明 650093；
3. 昆明理工大学 云南省有色金属真空冶金重点实验室，昆明 650093；
4. 昆明理工大学 复杂有色金属资源清洁利用国家重点实验室，昆明 650093

摘 要：利用热重分析仪(TGA) 在不同升温速率下对 CuSe 进行热分解实验。基于无模函数和有模函数分析，讨论 CuSe 分解的动力学参数和机理，并采用真空热重炉研究 CuSe 的分解速率和分解行为。结果表明，在目前的实验条件下，R3 是最可能的模型函数，其活化能和指前因子的平均值分别为 12.344 J/mol 和 0.152 s^{-1}。CuSe 的实际分解速率为 0.0030 g/(cm^2·min)。

关键词：CuSe；热分解；非等温动力学；机理

(Edited by Wei-ping CHEN)